

Effect of nuclear matter incompressibility on the $^{16}\text{O}+^{208}\text{Pb}$ system

O.N.Ghodsi*, F.Torabi

*Department of Physics, Faculty of Science, University of Mazandaran
P.O.Box 47415-416, Babolsar, Iran*

Abstract

To analyze the property of nuclear matter in the $^{16}\text{O}+^{208}\text{Pb}$ collision system, the internuclear potential of the fusion reaction is calculated by using the Skyrme forces associated with an extensive nuclear matter incompressibility K range in the semiclassical energy density formalism. Comparison of the experimental fusion cross sections and those obtained by using potentials derived from different forces with various K values shows that the incompressibility of nuclear matter changes during the fusion process at different bombarding energies. The results indicate that, as the energy increases, the nuclear matter becomes more incompressible.

*Email: o.ghodsi@umz.ac.ir

I. Introduction

Fusion in heavy-ion reactions has been one of the most extensively studied topics in nuclear physics over the last decades [1–14]. Various attempts have been made to explain this phenomenon by using a variety of theoretical models based on different assumptions. Taking into account the dynamical mechanism of the fusion process, the interaction potential between two nuclei can be determined by using dynamic approaches such as quantum molecular dynamics and time-dependent Hartree–Fock theory [15–20]. According to the frozen-density approximation, fusion reactions can be also analyzed by using static approaches such as the double-folding model and energy-density formalism [21–26]. By employing different effective nucleon-nucleon interactions in these models and methods, a large number of heavy-ion fusion reactions have been investigated in theoretical low-energy nuclear physics. Among them, the $^{16}\text{O}+^{208}\text{Pb}$ system is a candidate that has been widely studied by using static and dynamic approaches [27–30]. Some studies have shown that analysis of the fusion cross-section data of this heavy-ion reaction can help understand the importance of different factors in calculations of the interaction potential, including the energy dependence of the barrier [27] and the incompressibility of nuclear matter [30].

Nuclear matter incompressibility (K) is a key component of the nuclear matter equation of state (EOS) and has been one of the interesting subjects in studies of heavy-ion fusion reactions. Different versions of the effective interactions resulting in different K values have been used to investigate the role of nuclear matter incompressibility in heavy-ion fusion processes [30–32]. The results obtained revealed that theoretical fusion data is sensitive to the value of K . Therefore, describing the heavy-ion reaction by using different effective interactions with different K values may allow exploration of variations in the incompressibility of nuclear matter during the fusion process at different bombarding energies.

Accordingly, in the present study, we are motivated to examine this variation within the $^{16}\text{O}+^{208}\text{Pb}$ system. For this purpose, the interaction potential of the chosen system was calculated by using different Skyrme forces associated with K values ranging from 234 to 370 MeV in the semiclassical energy-density formalism. With respect to each force, the neutron and proton densities obtained by the self-consistent quantum-mechanical Hartree–Fock–Bogoliubov

(HFB) method were also employed in this formalism. Based on the best agreement achieved between the theoretical fusion cross sections obtained by the potentials derived from different forces and the experimental data, we have shown variation in the nuclear matter incompressibility within the $^{16}\text{O}+^{208}\text{Pb}$ system at different bombarding energies.

This paper is organized as follows: Section II introduces the Skyrme energy-density-functional model and describes the properties of the colliding nuclei based on the effective interactions employed in this model. Section III presents the calculations and results of analysis of the $^{16}\text{O}+^{208}\text{Pb}$ system by using different forces yielding various incompressibility values. Finally, Sec. IV draws the conclusions of this paper.

II. Theoretical Formalism

A. Semiclassical expression of the Skyrme energy-density functional

In the energy-density-functional model, the nuclear potential between the interacting nuclei, as a function of separation distance R , is given by

$$V_N(R) = E_T(R) - (E_1 + E_2), \quad (1)$$

$$E_T(R) = \int \mathcal{E} \left[\rho_{1p}(\vec{r}) + \rho_{2p}(\vec{r} - \vec{R}), \rho_{1n}(\vec{r}) + \rho_{2n}(\vec{r} - \vec{R}) \right] d^3r, \quad (2)$$

$$E_1 = \int \mathcal{E} [\rho_{1p}(\vec{r}), \rho_{1n}(\vec{r})] d^3r, \quad (3)$$

$$E_2 = \int \mathcal{E} [\rho_{2p}(\vec{r}), \rho_{2n}(\vec{r})] d^3r, \quad (4)$$

where E_1 and E_2 denote the energy of the noninteracting nuclei and $E_T(R)$ expresses the energy of the composite system. In these equations, the Skyrme energy density $\mathcal{E}(\vec{r})$ is defined as

$$\begin{aligned}
\mathcal{E}(\vec{r}) = & \frac{\hbar^2}{2m}\tau + \frac{1}{2}t_0 \left[\left(1 + \frac{1}{2}x_0\right) \rho^2 - \left(x_0 + \frac{1}{2}\right) (\rho_n^2 + \rho_p^2) \right] \\
& + \frac{1}{12}t_3\rho^\alpha \left[\left(1 + \frac{1}{2}x_3\right) \rho^2 - \left(x_3 + \frac{1}{2}\right) (\rho_n^2 + \rho_p^2) \right] \\
& + \frac{1}{4} \left[t_1 \left(1 + \frac{1}{2}x_1\right) + t_2 \left(1 + \frac{1}{2}x_2\right) \right] (\rho\tau) \\
& - \frac{1}{4} \left[t_1 \left(x_1 + \frac{1}{2}\right) - t_2 \left(x_2 + \frac{1}{2}\right) \right] (\rho_n\tau_n + \rho_p\tau_p) \\
& + \frac{1}{16} \left[3t_1 \left(1 + \frac{1}{2}x_1\right) - t_2 \left(1 + \frac{1}{2}x_2\right) \right] (\vec{\nabla}\rho)^2 \\
& - \frac{1}{16} \left[3t_1 \left(x_1 + \frac{1}{2}\right) + t_2 \left(x_2 + \frac{1}{2}\right) \right] [(\vec{\nabla}\rho_n)^2 + (\vec{\nabla}\rho_p)^2] \\
& + \frac{1}{2}W_0 \left[\vec{J} \cdot \vec{\nabla}\rho + \vec{J}_n \cdot \vec{\nabla}\rho_n + \vec{J}_p \cdot \vec{\nabla}\rho_p \right].
\end{aligned} \tag{5}$$

Here, $t_0, t_1, t_2, t_3, x_0, x_1, x_2, x_3, \alpha$ and W_0 are the Skyrme force parameters determined by fitting different properties of nuclei. m is the nucleon mass, and $\rho = \rho_n + \rho_p$, $\tau = \tau_n + \tau_p$, and $\vec{J} = \vec{J}_n + \vec{J}_p$ are the nuclear, kinetic, and spin-orbit densities, respectively. The kinetic energy and spin-orbit densities are estimated in the semiclassical extended Thomas–Fermi model (ETF).

Taking into consideration the \hbar^2 correction terms in this model, the functional form of the kinetic-energy density is given by ($q = n$ or p),

$$\begin{aligned}
\tau_q(\vec{r}) = & \frac{3}{5}(3\pi^2)^{\frac{2}{3}}\rho_q^{\frac{5}{3}} + \frac{1}{36} \frac{(\vec{\nabla}\rho_q)^2}{\rho_q} + \frac{1}{3}\Delta\rho_q + \frac{1}{6} \frac{\vec{\nabla}\rho_q \cdot \vec{\nabla}f_q}{f_q} + \frac{1}{6}\rho_q \frac{\Delta f_q}{f_q} - \frac{1}{12}\rho_q \left(\frac{\vec{\nabla}f_q}{f_q} \right)^2 \\
& + \frac{1}{2}\rho_q \left(\frac{2m}{\hbar^2} \right)^2 \left(\frac{W_0}{2} \frac{\vec{\nabla}(\rho + \rho_q)}{f_q} \right)^2,
\end{aligned} \tag{6}$$

where the effective mass form factor $f_q(\vec{r})$ takes the following form:

$$f_q(\vec{r}) = 1 + \frac{2m}{\hbar^2} \frac{1}{4} \left[t_1 \left(1 + \frac{x_1}{2}\right) + t_2 \left(1 + \frac{x_2}{2}\right) \right] \rho(\vec{r}) - \frac{2m}{\hbar^2} \frac{1}{4} \left[t_1 \left(x_1 + \frac{1}{2}\right) - t_2 \left(x_2 + \frac{1}{2}\right) \right] \rho_q(\vec{r}). \tag{7}$$

Because spin is intrinsically a quantum-mechanical property with no direct classical counterpart, the expression of (\vec{J}) in the ETF model is

$$\vec{J}_q(\vec{r}) = -\frac{2m}{\hbar^2} \frac{1}{2} W_0 \frac{1}{f_q} \rho_q \vec{\nabla}(\rho + \rho_q). \tag{8}$$

By using these equations, the nuclear part of the interaction potential, $V_N(R)$, is determined by knowledge of the density distributions of the projectile and target nuclei. Then, assuming that $\rho_{ch}^{(i)} \approx e\rho_p^{(i)}$, the Coulomb part is added to the calculations as

$$V_C(R) = \int \frac{\rho_{ch}^{(1)}(\vec{r}_1)\rho_{ch}^{(2)}(\vec{r}_2)}{|\vec{R} + \vec{r}_2 - \vec{r}_1|} d^3r_1 d^3r_2. \quad (9)$$

B. Properties of the interacting nuclei

To date, numerous parametrizations of the Skyrme effective interaction have been published and many of them have been applied in mean-field theories for a variety of purposes. In the present study, some of the available effective interactions that result in an EOS with an extensive range of K values are employed to study the nuclear matter incompressibility in the $^{16}\text{O}+^{208}\text{Pb}$ system. The selected forces are SkSC4 [33], Es [34], SKXce [35], E [34], and SI [36] with the incompressibility range between 234 and 370 MeV. Based on each force, the neutron and proton densities of the ^{16}O and ^{208}Pb nuclei were computed by using the microscopic HFB method because many properties of the finite nuclei can be described by this approximation. For instance, Fig. 1 shows the radial density distributions obtained from these calculations based on the SkSC4 and SI parameter sets.

By using the density distributions calculated in the HFB approach, it was found that all the selected Skyrme forces can reproduce the experimental binding energies and root-mean-square charge radii of the chosen nuclei with the relative deviations less than 4.69% and 2.88%, respectively. Figure 2 shows the percentage of relative deviations of the theoretical binding energies and root-mean-square charge radii from their corresponding experimental data for the SkSC4, Es, SKXce, E, and SI Skyrme forces. These effective forces, which can describe the ground-state properties of the ^{16}O and ^{208}Pb nuclei with reasonable accuracy, are applied to evaluate the nucleus-nucleus potential in the described energy-density-functional model.

III. Calculations and Results

To perform the calculations in the energy-density formalism, based on each of the selected

Skyrme forces, the two-parameter Fermi density distributions were determined by using the parameters obtained from fitting the results of HFB calculations. The calculated diffuseness parameters of the neutron- and proton-density distributions for the ^{16}O and ^{208}Pb nuclei are illustrated in Fig. 3 by using the SkSC4, Es, SKXce, E, and SI Skyrme forces. Employing the determined densities, together with their corresponding Skyrme interactions, we evaluated the interaction potential of the $^{16}\text{O}+^{208}\text{Pb}$ system. The characteristics of the calculated fusion barriers, i.e., barrier height and position, are displayed in Fig. 4 based on the Skyrme forces. The results clearly show that increasing the value of K , increases the fusion barrier height and decreases the value of the barrier position. Also, from Figs. 3 and 4, and due to the fact that surface nucleons play a significant role in heavy-ion reactions, one can find that the use of smaller diffuseness parameters in the density distributions decreases the attraction energy and consequently increases the barrier height.

By using the nucleus-nucleus potentials derived from different Skyrme forces we analyze here the fusion cross sections of the $^{16}\text{O}+^{208}\text{Pb}$ system in different energy ranges, i.e., below, near, and above the barrier. For this purpose, the cross-section data were calculated by using the CCFULL code [37], taking into account the excitations of 2^+ and 3^- states of the target and projectile nuclei. The parameters applied to describe the excitations of these low-lying states for the chosen nuclei were taken from Refs. [38, 39]. The results of the calculations based on the potentials obtained from the different forces are shown in Fig. 5 in both logarithmic and linear scales. It can be seen that the theoretical results are obviously influenced by the incompressibility of the Skyrme forces. The interaction potentials calculated from the forces with smaller incompressibility values precisely describe the experimental fusion cross sections [40] at low energies, but cannot explain the data at above-barrier energies. Furthermore, it is evident that the potentials obtained from the forces associated with higher incompressibility values can accurately reproduce the fusion cross sections at high energies; however, they cannot predict the data at subbarrier energies. To be more precise, based on this observation, it is found that the Skyrme forces associated with the nuclear incompressibility values $\sim 234\text{--}248$ MeV can reproduce the fusion cross sections of $^{16}\text{O}+^{208}\text{Pb}$ at energies below and near the barrier, the Skyrme force resulting in $K=270$ MeV can explain the experimental data at energies in the vicinity and nearly above

the barrier, and the forces leading to $K > 300$ MeV can be used to predict the fusion cross sections at energies above the barrier and at higher energies.

To demonstrate the importance of the density parameters in these calculations, the fusion cross sections of the chosen system were also computed by using the potentials derived from the different forces and the same sets of density parameters, which were obtained with the SkP Skyrme force [41] for the interacting nuclei. The calculated fusion cross sections are illustrated in Fig. 6. As one can observe, in this case, the experimental and theoretical fusion cross sections are not in agreement, which clearly shows that the density parameters play a key role in reproducing the experimental fusion data and in examining the sensitivity of the fusion cross sections to the incompressibility value at different bombarding energies.

In addition, to study the nuclear matter incompressibility in the $^{16}\text{O} + ^{208}\text{Pb}$ system, the fusion barrier distribution, $d^2(E\sigma_{fus})/dE^2$, for this system was computed. Figure 7 shows the barrier distributions calculated by using the cross sections derived from different Skyrme forces. The theoretical barrier distributions display almost a similar behavior as found in the prediction of the fusion cross sections. The experimental representation of the barrier distribution at high energies can be better explained by using the cross sections derived from the Skyrme forces yielding higher K values. However, at low energies, the agreement between the experimental and theoretical barrier distributions is achieved by using the data computed from the forces with smaller values for K .

According to the results, one can indicate the variation in the nuclear-matter incompressibility within the $^{16}\text{O} + ^{208}\text{Pb}$ system at different energies. To illustrate this, based on the best agreement achieved between the calculated and experimental fusion cross sections at each energy, the predicted values of the nuclear incompressibility at different bombarding energies are displayed in Fig. 8. As seen, the incompressibility of the nuclear matter increases by increasing the bombarding energy.

At each energy, the corresponding temperature T of the compound nucleus, which is displayed on the top horizontal axis of this figure, was calculated by the following formula [42, 43]:

$$E^* = E_{c.m.} + Q_{in} = \frac{1}{a}AT^2 - T, \quad (10)$$

where, E^* , $E_{c.m.}$, and Q_{in} are the excitation energy of the compound nucleus, the center-of-mass energy of the projectile nucleus, and the entrance-channel Q value, respectively. Moreover, in this equation $a = 9$ or 10 for intermediate mass or superheavy systems.

It can be observed that, by increasing the bombarding energy, the temperature of the compound nucleus increases as well. Therefore, one can expect a variation in the mean-field of the compound system and, consequently, in the property of the nuclear matter as the bombarding energy increases.

Efficiency of the described method for other systems

By using the suitable Skyrme forces and their corresponding density distributions, the described method can be also applied to study the incompressibility of nuclear matter in other fusion reactions. To show the efficiency of this method for other systems, we briefly discuss the results of the theoretical fusion cross sections for the $^{40}\text{Ca}+^{90}\text{Zr}$ system.

The potentials derived from the SkT4, SkT1*, SK255, and SK272 Skyrme forces [44,45], which yield the K values in the range between 235 and 272 MeV and can reasonably describe the properties of the interacting nuclei, were selected as the best choices to describe the fusion cross sections of the system at different bombarding energies. By using these potentials, the theoretical fusion cross sections of the $^{40}\text{Ca}+^{90}\text{Zr}$ system were computed with the CCFULL code. Figure 9 compares the theoretical results with the experimental data [46]. The agreement between the experimental and theoretical fusion cross sections derived from the forces with different incompressibility values shows that, as the bombarding energy increases, the nuclear matter becomes more incompressible.

IV. Conclusions

The present study examined the variation in the incompressibility of nuclear matter in the $^{16}\text{O}+^{208}\text{Pb}$ fusion reaction. To this end, the interaction potential of the system was calculated by using different Skyrme interactions with the K values ranging from 234 to 370 MeV in the energy-density formalism. Analysis of the potentials indicated that the use of Skyrme forces with higher nuclear incompressibility values results in greater barrier

heights whose corresponding positions are shifted to closer distances between the interacting nuclei. The fusion cross sections of the chosen system were computed by using the ion-ion potentials and the CCFULL code. The results revealed that the experimental cross sections at subbarrier energies can be accurately described by the potentials derived from the forces with smaller K values. On the other hand, the data at higher energies can be satisfactorily explained by the potentials obtained from the forces associated with higher K values. This trend suggests that an exact fit to fusion cross-section data in different energy ranges can be achieved by using forces with different incompressibility values.

Based on the calculations made by the Skyrme energy density formalism and the CC-FULL code, one can conclude that nuclear matter during the fusion process changes from less-incompressible matter at low energies to more-incompressible matter at higher energies. In addition, it is worth mentioning that the applied method enables analysis of the property of nuclear matter in the fusion process at different bombarding energies based on a static model.

References

- [1] C. H. Dasso, S. Landowne, and A. Winther, Nucl. Phys. A **405**, 381(1983).
- [2] T. Udagawa, B. T. Kim, and T. Tamura, Phys. Rev. C **32**, 124 (1985).
- [3] N. Rowley, G. R. Satchler, and P. H. Stelson, Phys. Lett. B **254**, 25 (1991).
- [4] W. Reisdorf, J. Phys. G **20**, 1297 (1994).
- [5] V. Yu. Denisov and S. Hofmann, Phys. Rev. C **61**, 034606 (2000).
- [6] C. H. Dasso and G. Pollarolo, Phys. Rev. C **68**, 054604 (2003).
- [7] C. L. Jiang, B. B. Back, H. Esbensen, R. V. F. Janssens, and K. E. Rehm, Phys. Rev. C **73**, 014613 (2006).
- [8] Z. Q. Feng, G. M. Jin, and F. S. Zhang, Nucl. Phys. A **802**, 91 (2008).
- [9] T. Ichikawa, K. Hagino, and A. Iwamoto, Phys. Rev. Lett. **103**, 202701 (2009).
- [10] I. Dutt and R. K. Puri, Phys. Rev. C **81**, 047601 (2010).
- [11] S. Ayik, B. Yilmaz, and D. Lacroix, Phys. Rev. C **81**, 034605 (2010).
- [12] V. V. Sargsyan, G. G. Adamian, N. V. Antonenko, W. Scheid, and H. Q. Zhang, Phys. Rev. C **84**, 064614 (2011).
- [13] K. Hagino and N. Takigawa, Prog. Theor. Phys. **128**, 1061 (2012).
- [14] M. S. Gautam, Nucl. Phys. A **933**, 272 (2015).
- [15] A. S. Umar and V. E. Oberacker, Phys. Rev. C **74**, 021601 (2006).
- [16] K. Washiyama and D. Lacroix, Phys. Rev. C **78**, 024610 (2008).
- [17] C. Simenel and B. Avez, Int. J. Mod. Phys. E **17**, 31 (2008).
- [18] J. Aichelin and H. Stöcker, Phys. Lett. B **176**, 14 (1986).
- [19] J. Aichelin, Phys. Rep. **202**, 233 (1991).

- [20] N. Wang, Z. Li, and X. Wu, Phys. Rev. C **65**, 064608 (2002).
- [21] G. R. Satchler and W. G. Love, Phys. Rep. **55**, 183 (1979).
- [22] L. C. Chamon, G. P. A. Nobre, D. Pereira, E. S. Rossi, Jr., C. P. Silva, L. R. Gasques, and B. V. Carlson Phys. Rev. C **70**, 014604 (2004).
- [23] I. I. Gontchar, D. J. Hinde, M. Dasgupta, and J. O. Newton, Phys. Rev. C **69**, 024610 (2004).
- [24] R. K. Puri and R. K. Gupta, Phys. Rev. C **45**, 1837 (1992).
- [25] V. Yu. Denisov, Phys. Lett. B **526**, 315 (2002).
- [26] M. Liu, N. Wang, Z. Li, X. Wu, and E. Zhao, Nucl. Phys. A **768**, 80 (2006).
- [27] A. S. Umar, C. Simenel, and V. E. Oberacker, Phys. Rev. C **89**, 034611 (2014).
- [28] A. S. Umar and V. E. Oberacker, Eur. Phys. J. A **39**, 243 (2009).
- [29] K. Hagino and Y. Watanabe, Phys. Rev. C **76**, 021601 (2007).
- [30] H. Esbensen and Ş. Mişicu, Phys. Rev. C **76**, 054609 (2007).
- [31] Ş. Mişicu and H. Esbensen, Phys. Rev. Lett. **96**, 112701 (2006).
- [32] Ş. Mişicu and H. Esbensen, Phys. Rev. C **75**, 034606 (2007).
- [33] Y. Aboussir, J. M. Pearson, A. K. Dutta, and F. Tondeur, Nucl. Phys. A **549**, 155 (1992).
- [34] J. Friedrich and P.-G. Reinhard, Phys. Rev. C **33**, 335 (1986).
- [35] B. A. Brown, Phys. Rev. C **58**, 220 (1998).
- [36] D. Vautherin and D. M. Brink, Phys. Rev. C **5**, 626 (1972).
- [37] K. Hagino, N. Rowley, and A.T. Kruppa, Comput. Phys. Commun. **123**, 143 (1999).
- [38] S. Raman, C. W. Nestor Jr., and P. Tikkanen, At. Data Nucl. Data Tables **78**, 1 (2001).

- [39] T. Kibedi and R. H. Spear, *At. Data Nucl. Data Tables* **80**, 35 (2002).
- [40] C. R. Morton, A. C. Berriman, M. Dasgupta, D. J. Hinde, J. O. Newton, K. Hagino, and I. J. Thompson, *Phys. Rev. C* **60**, 044608 (1999).
- [41] J. Dobaczewski, H. Flocard, and J. Treiner, *Nucl. Phys. A* **422**, 103 (1984).
- [42] R. K. Puri and R. K. Gupta, *J. Phys. G* **18**, 903 (1992).
- [43] R. K. Gupta, S. Singh, R. K. Puri, A. Sandulescu, W. Greiner, and W. Scheid, *J. Phys. G* **18**, 1533 (1992).
- [44] F. Tondeur, M. Brack, M. Farine, and J. M. Pearson, *Nucl. Phys. A* **420**, 297 (1984).
- [45] B. K. Agrawal, S. Shlomo, and V. Kim Au, *Phys. Rev. C* **68**, 031304 (2003).
- [46] H. Timmers, D. Ackermann, S. Beghini et al., *Nuclear Physics, A* **633**, 421 (1998).

FIGURE CAPTIONS

Fig. 1. The neutron and proton density distributions of (a) the ^{16}O and (b) ^{208}Pb nuclei obtained by using the SkSC4 and SI Skyrme interactions in the HFB approximation.

Fig. 2. The percentage relative deviations, i.e., $|(Theo. - Exp.)/Exp.| \times 100$, of (a) the theoretical binding energies and (b) root-mean-square charge radii from their experimental data for the ^{16}O and ^{208}Pb nuclei. The incompressibility values corresponding to the Skyrme forces are displayed on the top horizontal axis.

Fig. 3. The calculated diffuseness parameters of the neutron and proton density distributions, $a_{n,p}$, for (a) the ^{16}O and (b) ^{208}Pb nuclei. The incompressibility values corresponding to the Skyrme forces are displayed on the top horizontal axis.

Fig. 4. (a) The theoretical fusion barrier heights and (b) positions calculated from different Skyrme forces for the $^{16}\text{O}+^{208}\text{Pb}$ system. The incompressibility values corresponding to the Skyrme forces are displayed on the top horizontal axis.

Fig. 5. The fusion cross sections of the $^{16}\text{O}+^{208}\text{Pb}$ system calculated with the potentials obtained from different Skyrme forces. The experimental data were taken from Ref. [40].

Fig. 6. The fusion cross sections of the $^{16}\text{O}+^{208}\text{Pb}$ system calculated with the potentials derived from different Skyrme forces and the density parameters obtained from the SkP Skyrme force.

Fig. 7. The fusion barrier distributions for the $^{16}\text{O}+^{208}\text{Pb}$ system calculated by using the cross sections derived from different Skyrme forces and their corresponding density distributions.

Fig. 8. The predicted values of the nuclear matter incompressibility in the $^{16}\text{O}+^{208}\text{Pb}$ system at different bombarding energies. The temperature of the compound nucleus corresponding to each energy is displayed on the top horizontal axis.

Fig. 9. The fusion cross sections of the $^{40}\text{Ca}+^{90}\text{Zr}$ system calculated with the potentials obtained from the SkT4, SkT1*, SK255, and SK272 Skyrme forces and their corresponding density distributions. The experimental data were taken from Ref. [46].

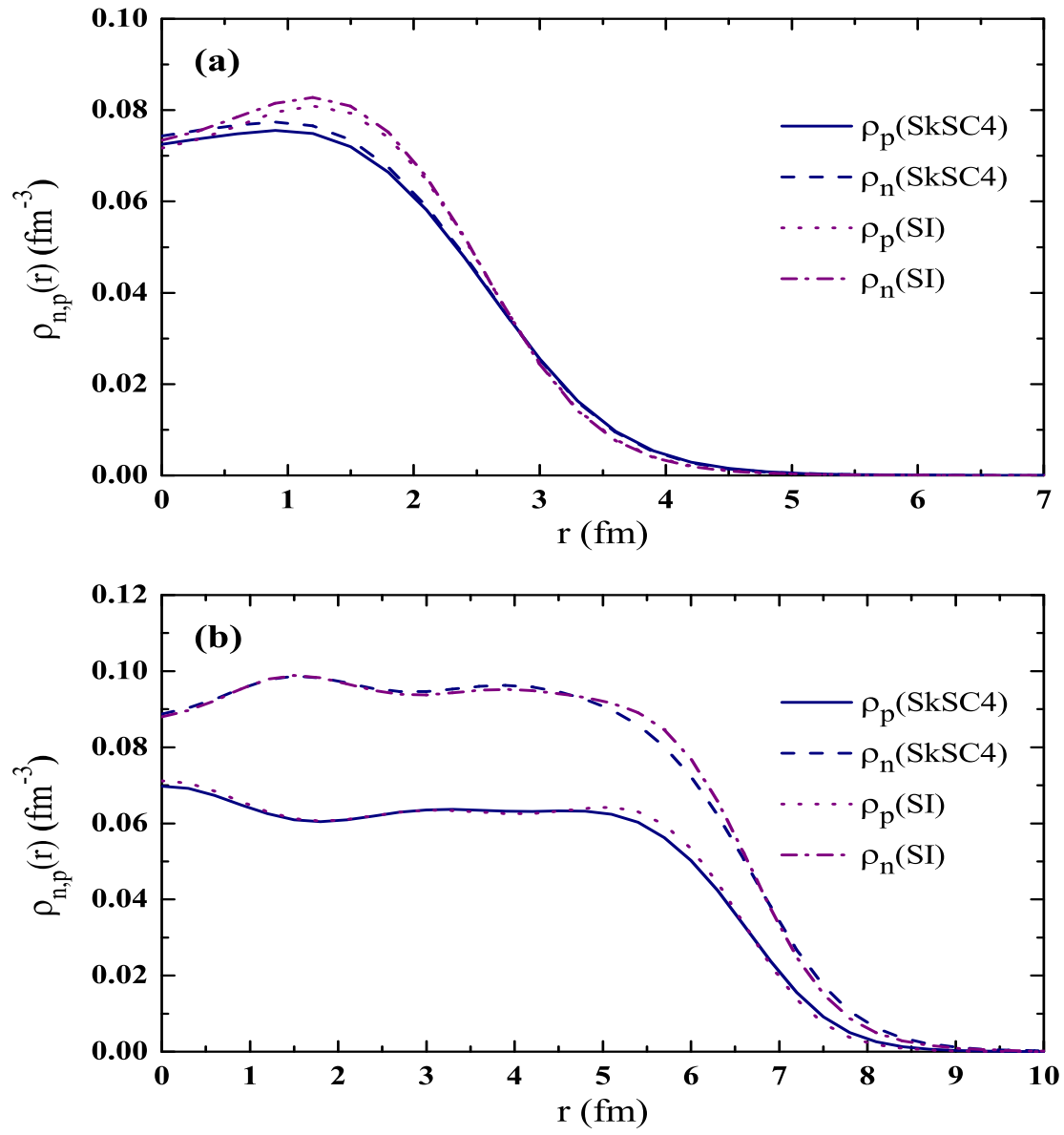


Figure 1:

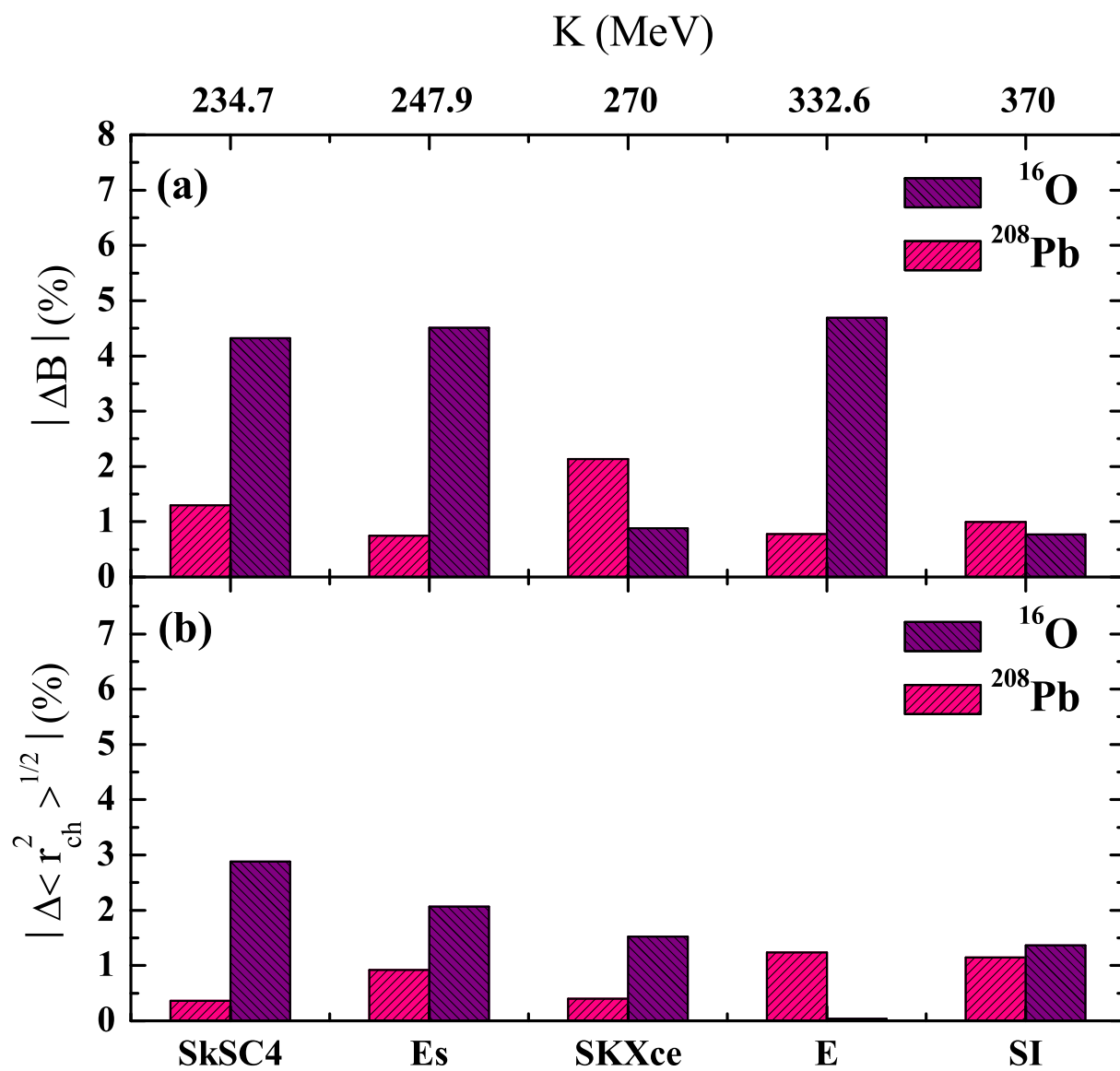


Figure 2:

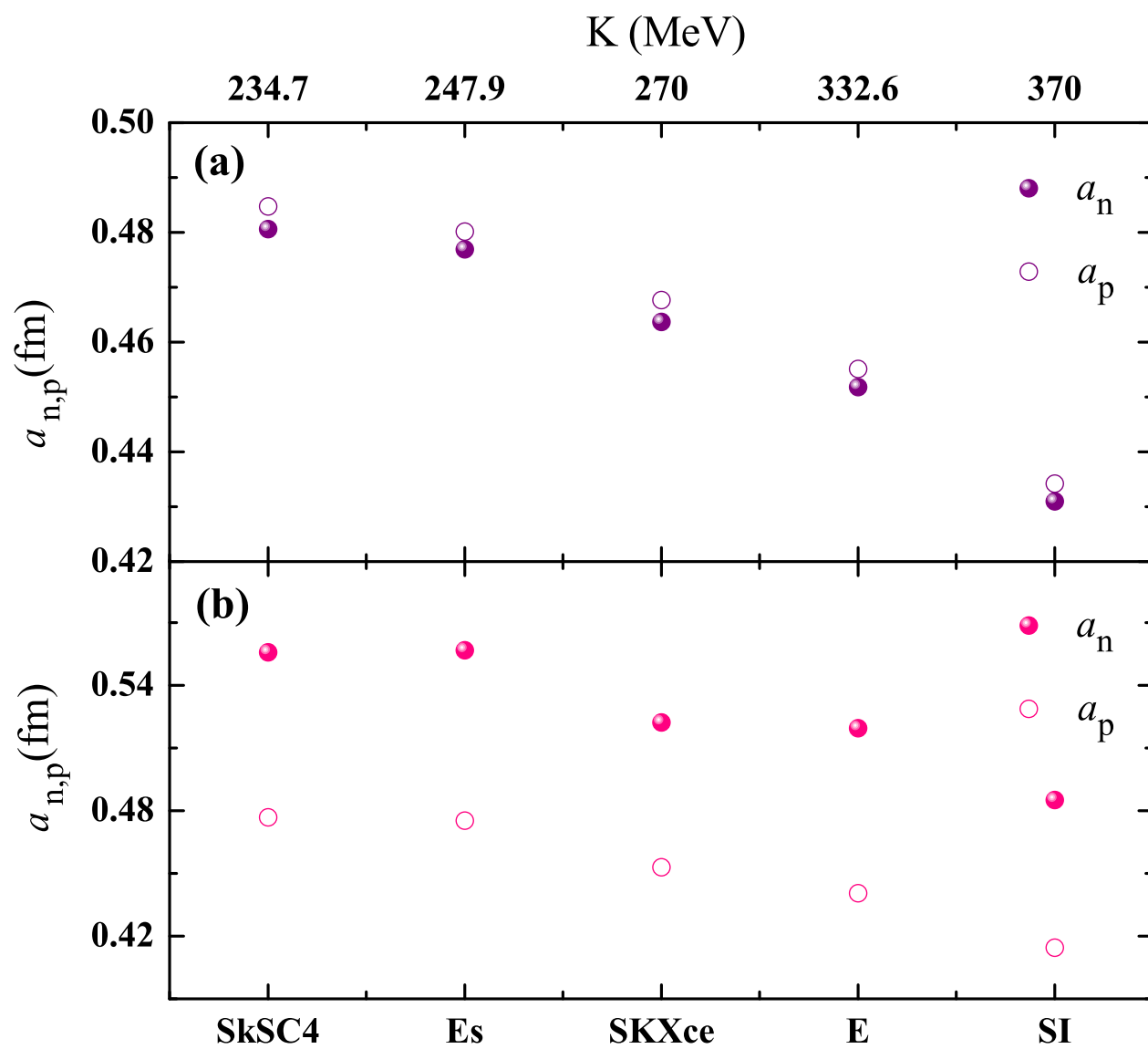


Figure 3:

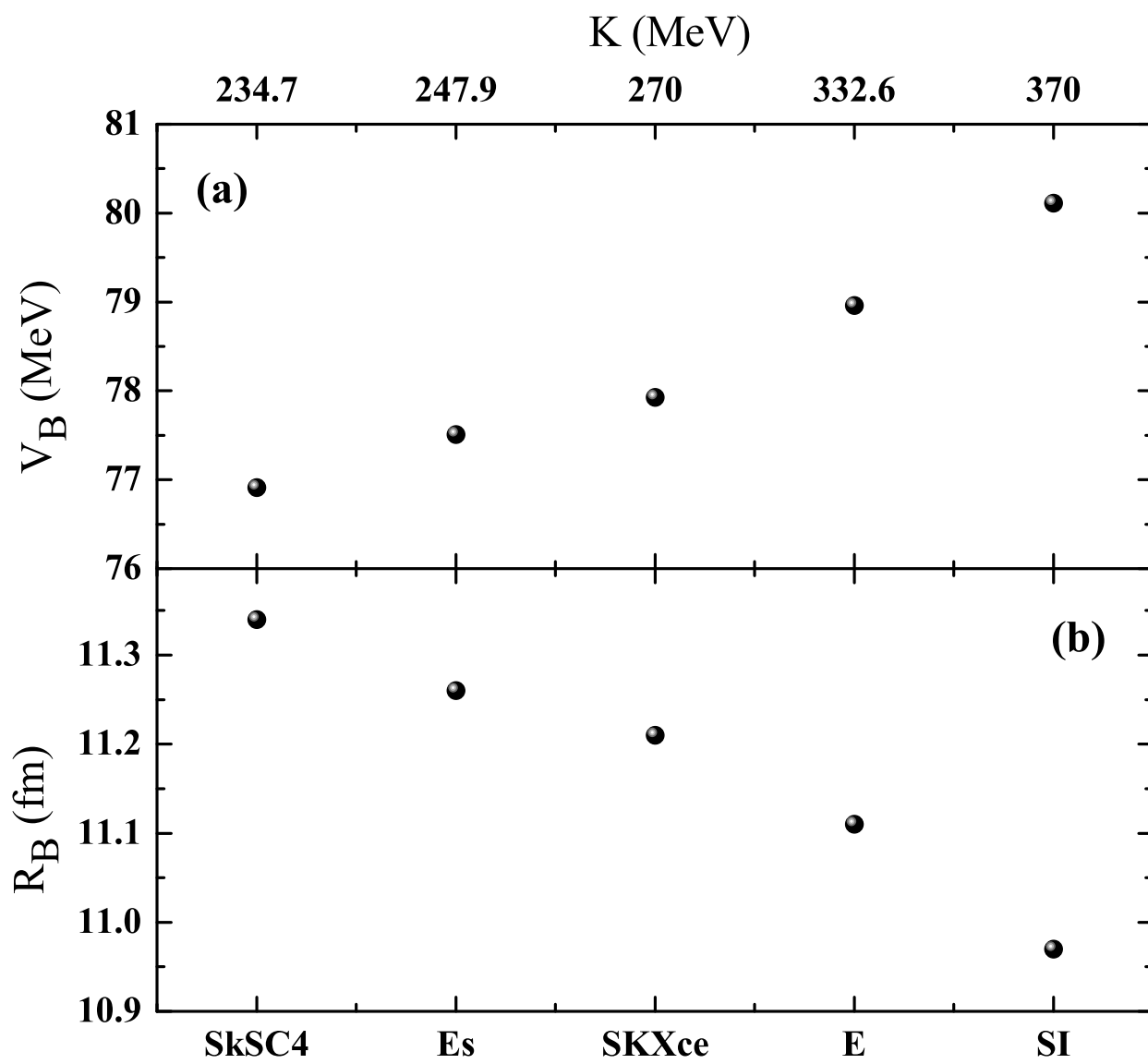


Figure 4:

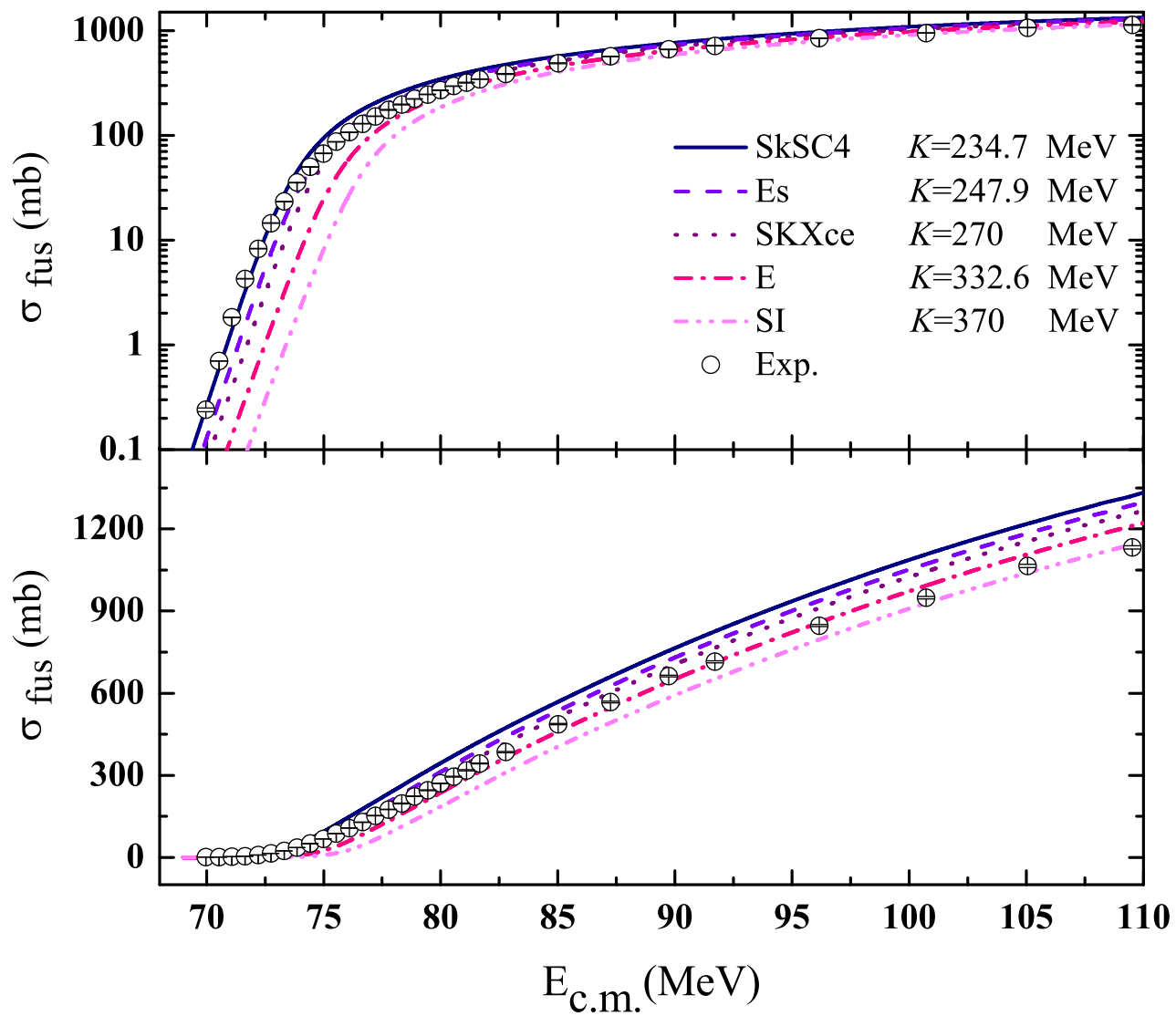


Figure 5:

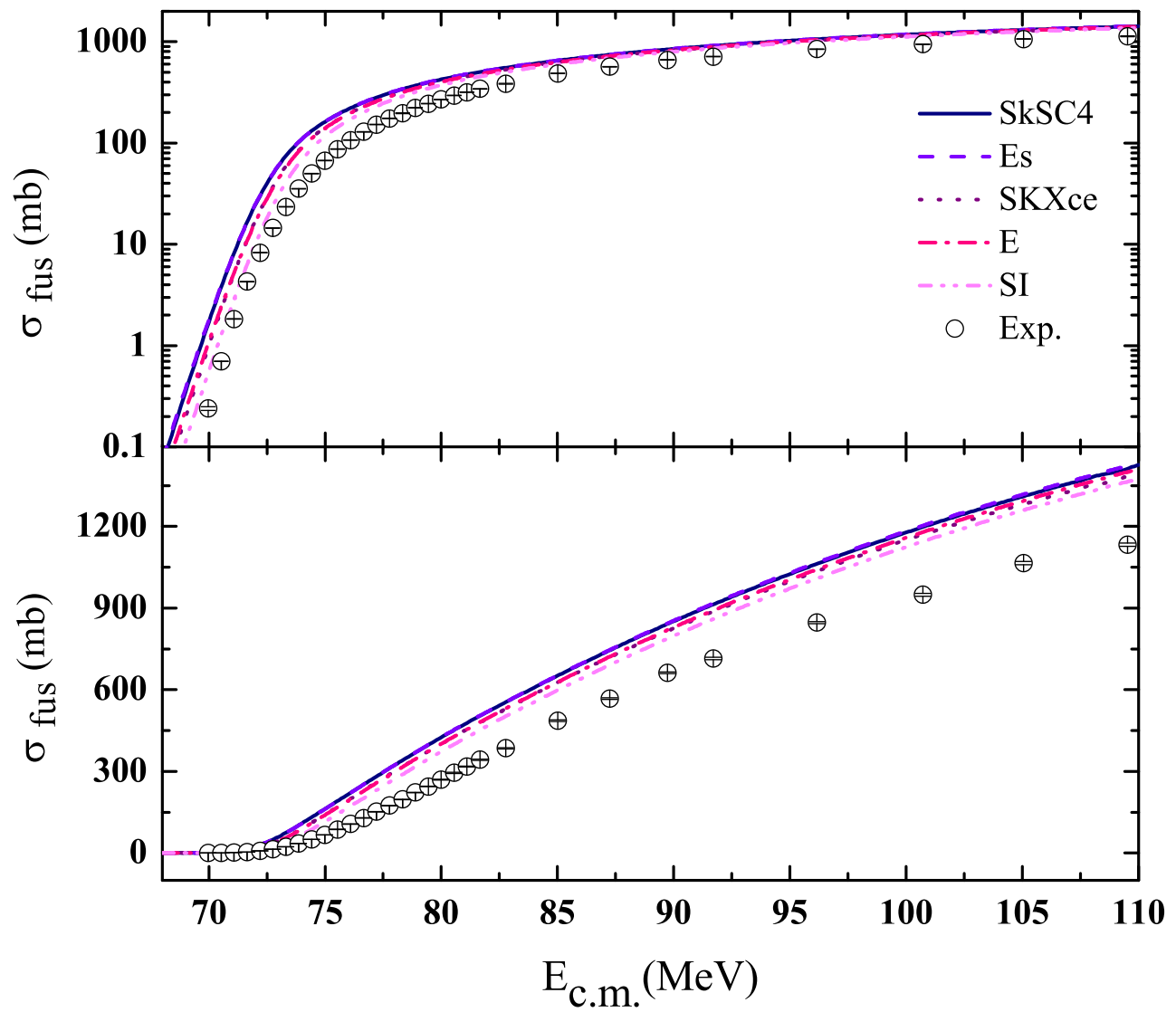


Figure 6:

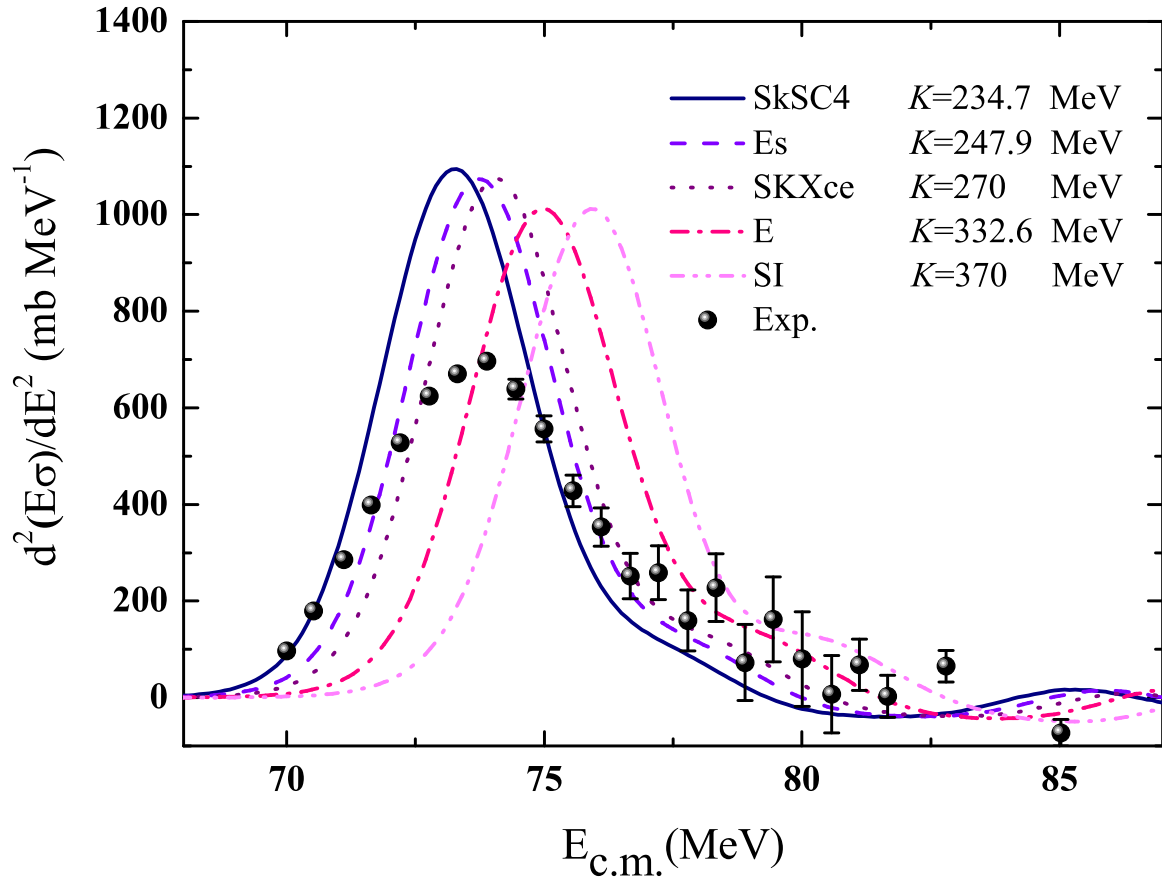


Figure 7:

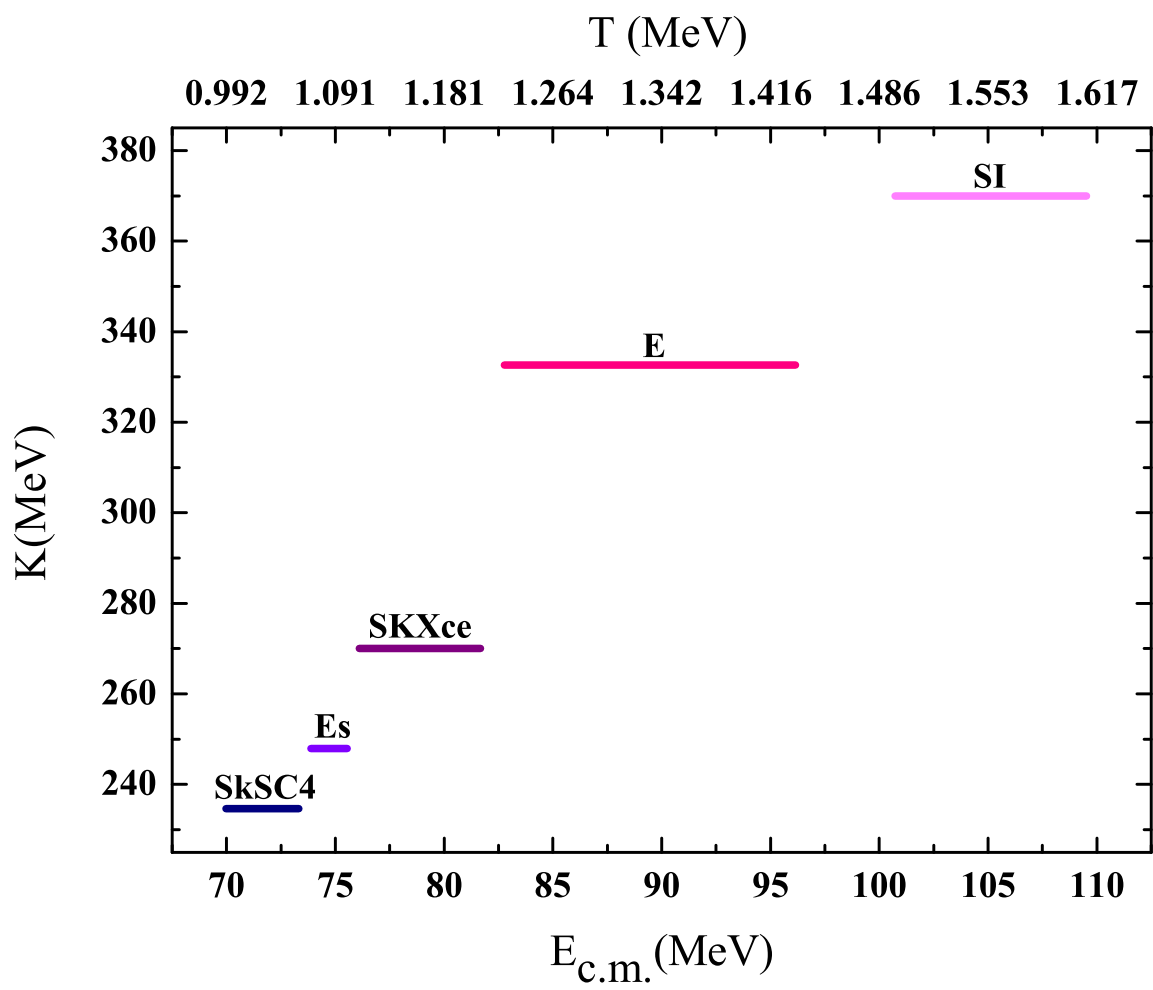


Figure 8:

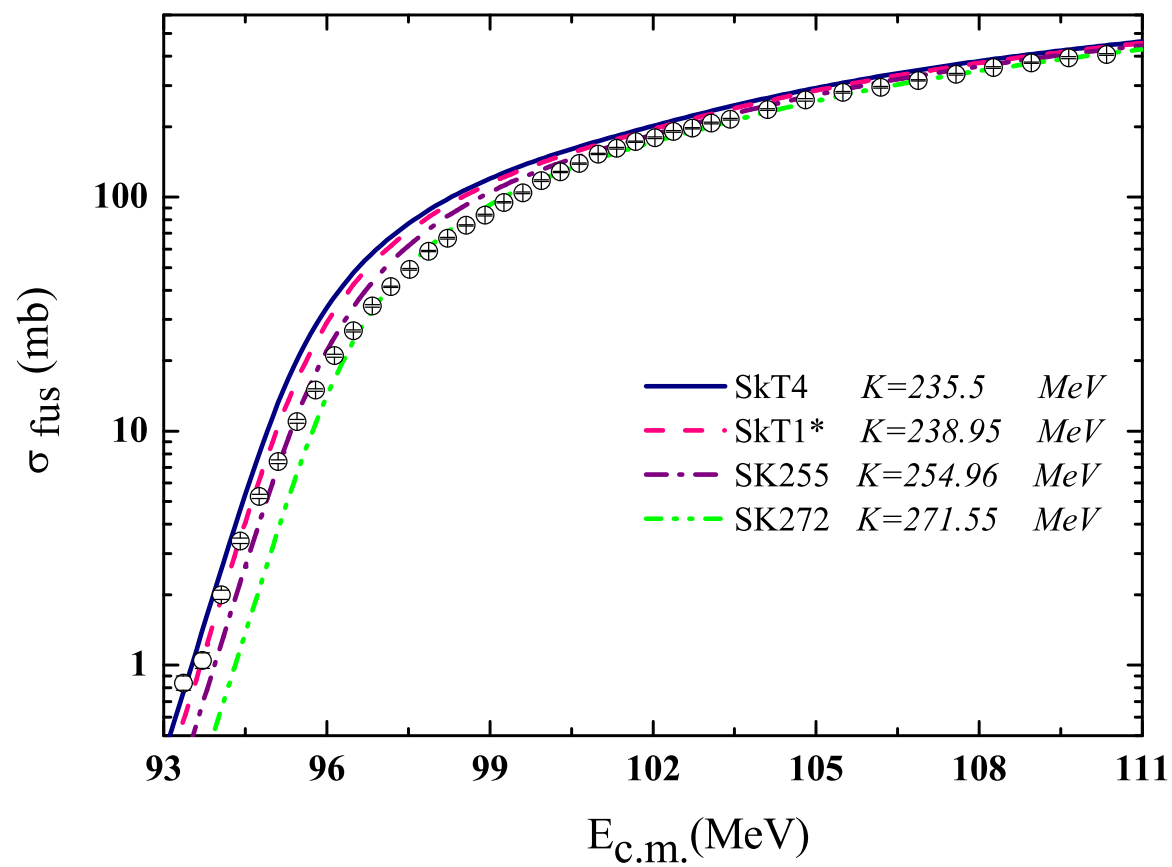


Figure 9: